Anomalous Cosmic Ray Modulation in the Heliosheath

R. D. Strauss*, M. S. Potgieter*, S. E. S. Ferreira* and M. E. Hill†

*Unit for Space Physics, North-West University, Potchefstroom, South Africa.
†Applied Physics Laboratory, Johns Hopkins University, Laurel, Maryland, USA.

Abstract. **After the Voyager 1 and 2 crossings of the solar wind termination shock (TS), the focus on anomalous cosmic ray (ACR) modulation has shifted to improving our basic understanding of how and where exactly the ACRs are accelerated in the heliosheath. This study is focused on two prominent additional modulation effects in this region: adiabatic heating and stochastic acceleration. Using a comprehensive TS model, the effects of these processes on the modulation of ACR Oxygen are studied and compared to diffusive shock acceleration. It is illustrated how these mechanisms play a role and to what energy range they are effective, depending on the assumed solar wind profile and other features of the heliosheath. Comparisons are made to recent Voyager 1 cosmic ray Oxygen observations.**

Keywords**: Anomalous Cosmic Rays, Stochastic Acceleration, Heliosheath, Termination Shock.**

I. INTRODUCTION

Previous modulation studies (e.g. [5] and [13]) have shown that adiabatic heating occuring in the heliosheath may account for the observed increase (e.g. [12]) in ACR intensities past the TS. Also, [3] have shown that stochastic acceleration (diffusion in momentum space) can reproduce the observed spectral shape of ACRs in the heliosheath. In this study, we further investigate the effect of these processes on the modulation of ACR Oxygen (O*). See also the accompanying papers, [9] and [10], this conference.

II. MODULATION MODEL

Stochastic acceleration is incorporated, through the last term in Eq. 1, into the Parker transport equation in the form (e.g. [8])

$$\frac{\partial f}{\partial t} = -\left(\vec{V} + \langle \vec{v_D} \rangle\right) \cdot \nabla f + \nabla \cdot \left(\vec{K_s} \cdot \nabla f\right) + \frac{1}{3}\left(\nabla \cdot \vec{V}\right) \frac{\partial f}{\partial \ln P} + \frac{1}{P^2}\frac{\partial}{\partial P}\left(P^2 K_P \frac{\partial f}{\partial P}\right). \quad (1)$$

This equation is solved numerically to obtain the omni-directional O* distribution function f, in terms of radial distance r, polar angle θ and particle rigidity P. $\vec{K}$ is the diffusion tensor, with $K_{\perp,\theta/r}$ and K_D taken from [1] and $K_{||}$ from [2], based on the results of [11], for protons. Under the assumption that the magnetic field variance scales as $\delta B^2 \sim B^2$ in the heliosheath, $K_{||}$ scales roughly as $K_{||} \sim 1/B$ in this region. K_P is the momentum diffusion coefficient, to be discussed later.

As discussed in [9], the TS compression ratio $s(\theta)$ and the ACR injection efficiency is scaled as a function of polar angle, resulting a region of preferred acceleration in the nose direction of the heliosphere. Also discussed in [9], the following solar wind velocity $\vec{V}_{sw}(r,\theta)$ decrease is assumed in the heliosheath

$$\vec{V}_{sw} \propto \left[\frac{r}{r_{TS}}\right]^{a(r)} \vec{\mathbf{e}}_r, \quad (2)$$

with $a(r_{TS}) = -2$ at the TS ($r_{TS} = 94$ AU), but decreasing to $a(r_{HP}) = -6$ at the heliopause ($r_{HP} = 140$ AU). As discussed in the rest of the text, this form of $\vec{V}_{sw}$ has a large effect on all modulation parameters in the outer heliosheath. The magnetic field $\vec{B}(r,\theta)$, for instance, increases as $B \sim 1/(rV_{sw})$ in the heliosheath. $\vec{V}_{sw}$ and $\vec{B}$ are shown in Fig. 1a as a function of radial distance. As discussed in [9], this form of $\vec{V}_{sw}$ has a non-zero divergence ($\nabla \cdot \vec{V}_{sw} < 0$, see [9]) in the heliosheath, leading to adiabatic heating in this region.

The solar wind number density $\rho_n(r,\theta)$, is calculated throughout the heliosphere by making use of the conservation of momentum flux

$$\rho_n(r,\theta) = \rho_n(r_E, 90^o)\left[\frac{r_E}{r}\right]^2 \left[\frac{V_{sw}(r_E, 90^o)}{V_{sw}(r,\theta)}\right], \quad (3)$$

with $r_E = 1$ AU, $\rho_n(r_E, 90^o) = 5$ particles.cm^{-3} and $V_{sw}(r_E, 90^o) = 400$ km.s^{-1}. From this, the Alvén speed is calculated as

$$V_A(r,\theta) = \frac{B(r,\theta)}{\sqrt{\mu_0 \rho_m(r,\theta)}}, \quad (4)$$

with $\rho_m(r,\theta) = \rho_n(r,\theta) m_p$ the solar wind mass density. Close to the Sun, $B \sim r^{-2}$ resulting in $V_A \sim 1/r$, but as $r \gg 1$ AU, $B \sim 1/r$ and V_A assumes a constant value up to the TS. Across the TS, V_A increases by a factor of $\sqrt{s(\theta)}$ and as $V_A \sim 1/\sqrt{V_{sw}}$ into the heliosheath. Using Eq. 2 this translates to a $V_A \sim r$ increase near the TS, but steepening to $V_A \sim r^3$ near the HP. V_A and ρ_n is shown as a function of radial distance in Fig. 1b.

The momentum diffusion coefficient K_P, is defined as the pitch angle averaged Fokker-Planck momentum diffusion coefficient ([7])

$$K_P \equiv \int_{-1}^{1} D_{PP} d\mu. \quad (5)$$

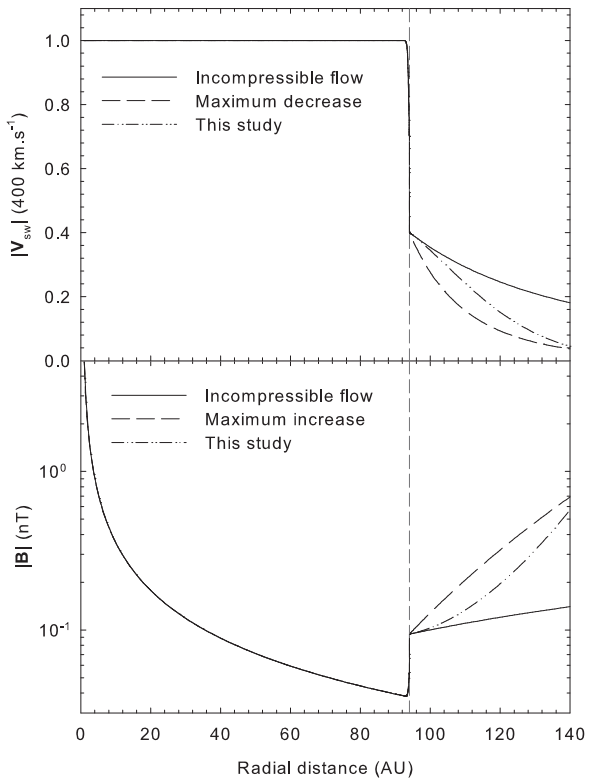

(a) The solar wind speed ($|\vec{V_{sw}}|$, top panel) and heliospheric magnetic field strength ($|\vec{B}|$, bottom panel) as a function of radial distance.

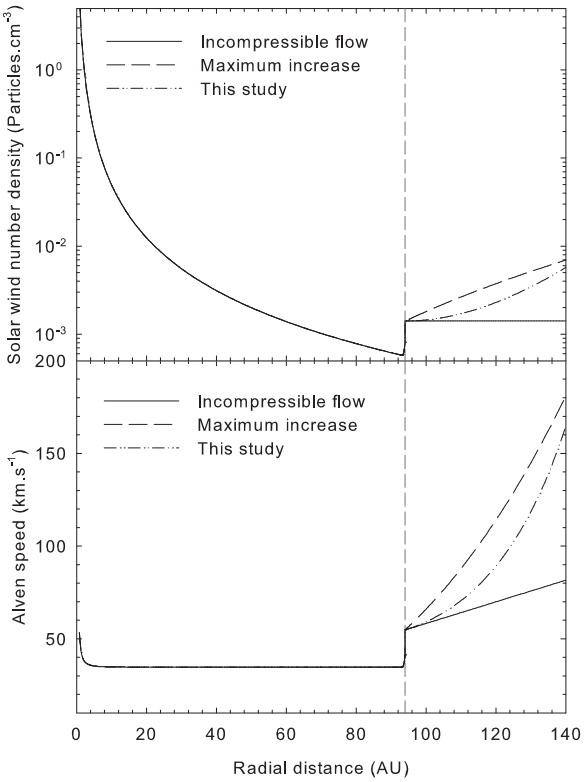

(b) The solar wind number density (ρ_n, top panel) and Alvén speed (V_A, bottom panel) as a function of radial distance.

Fig. 1: Various heliospheric parameters shown as a function of radial distance. Three different cases are shown, namely incompressible flow ($V_{sw} \sim r^{-2}$), the decrease according to Eq. 2, as well as an assumed maximum decrease (or in some cases an increase) of $V_{sw} \sim r^{-6}$. The TS position is indicated by the vertical dashed line.

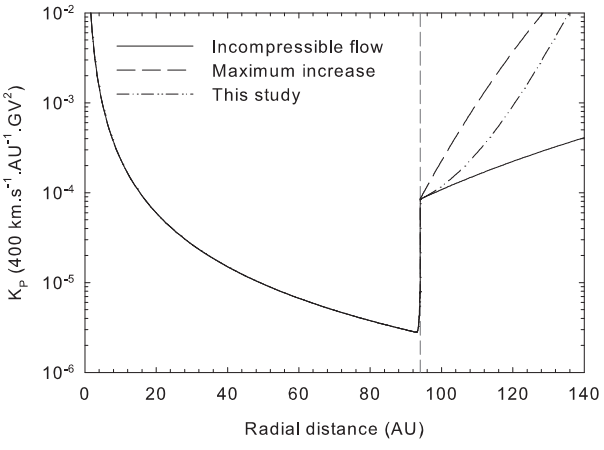

(a) K_P as a function of radial distance.

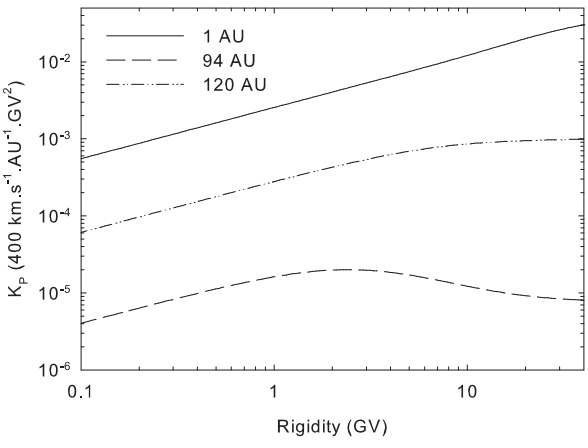

(b) K_P as a function of rigidity.

Fig. 2: The momentum diffusion coefficient K_P, shown as a function of radial distance (left panel) at a rigidity of 1 GV, in the equatorial plane. The different profiles correspond to those shown in Fig. 1. The right panel shows K_P as a function of rigidity at radial distances of 1, 94 and 120 AU, in the equatorial plane.

To obtain a workable expression for K_P we use the results of [8], from which we obtain

$$K_P = K_{P,0} \frac{P^2 V_A^2(r,\theta)}{K_{||}(r,\theta,P)}, \qquad (6)$$

with $K_{P,0}$ a dimensionless constant, (only dependent on the Kolmagorov inertial turbulence spectrum index, $k =$

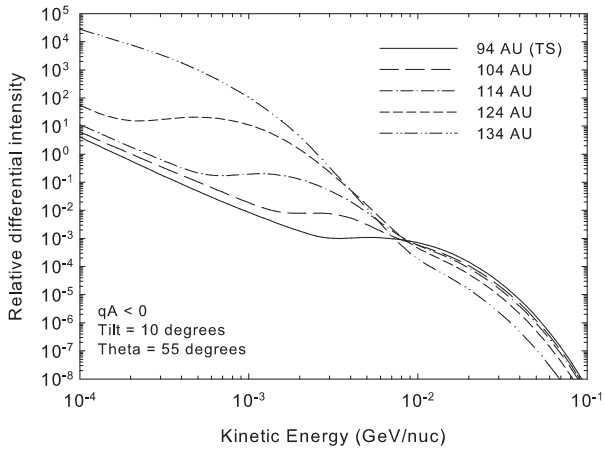

Fig. 3: The modeled O* energy spectra in the heliosheath at a polar angle of 55^o for the qA < 0 magnetic polarity cycle. Spectra are shown at the TS (94 AU), and then at 10 AU intervals into the heliosheath. The HP is located at 140 AU.

$5/3$) given by

$$K_{P,0} = \frac{1}{k(2+k)(2-k)(4-k)} \approx \frac{1}{5}, \qquad (7)$$

assuming a vanishing magnetic field helicity. However, $K_{||}$ from [8] and [2], although being very similar, are not exactly of the same form. For the lack of a better approximation, we assume the functional form of Eq. 6, but we take $K_{P,0} \in \{0, 1\}$ to be a free parameter [13]. Using $K_{P,0} = 1/2$, K_P is shown as a function of radial distance and rigidity in Fig. 2. Note the large values of K_P in the outer heliosheath, as K_P increases across the TS by a factor of $s^2(\theta)$, and as $K_P \sim 1/(rV_{sw}^2)$ into the heliosheath. We thus have a $K_P \sim r^3$ increase at the TS, steepening to $K_P \sim r^{11}$ at the HP, using Eq. 2.

III. Results

The Voyager 1 Oxygen intensities (as shown in Figs. 4 and 5) are measured by the Low Energy Charged Particle (LECP) instrument package ([4]) on board the Voyager 1 spacecraft, which includes a solid state detector (SSD) telescope. Clean elemental separation results from comparing kinetic energy deposits in two adjacent SSDs and here we use measurements averaged over LECP field of view.

Fig. 3 shows the modeled energy spectra of O* in the heliosheath. The spectra are shown for the qA < 0 polarity cycle, for solar minimum conditions (assumed current sheet tilt angle of 10^o) at a polar angle of 55^o. The spectra are shown at a radial distance of 94 AU (the assumed position of the TS) and at 10 AU intervals up to the HP (140 AU). Recall from Fig. 2, the very high values of K_P near the HP, allowing for very efficient momentum diffusion taking place in this region. O* accelerated through diffusive shock acceleration at the TS, are transported into the heliosheath where they experience adiabatic heating and stochastic acceleration. These re-accelerated O* then diffuse back towards the TS, resulting in the modulated spectral shapes in the heliosheath, shown in Fig. 3.

Fig. 4 is similar to Fig. 3, but here the modeled spectra are compared to Voyager 1 O* observations. The modeled spectra are shown at radial distances of 89, 94, 99, 104 and 109 AU. See the figure caption for details on the data set. Note the large effect from stochastic acceleration in the energy range $1 - 10$ MeV.nuc^{-1}, where a significant increase in intensity past the TS is both modeled and observed. Also note that the energy where the flattening of the spectra is observed, changes from ~ 3 MeV.nuc^{-1} at 94 AU to ~ 1 MeV.nuc^{-1} at 109 AU, thus moving to lower energies.

Fig. 5 shows both the computed and observed O* intensities as a function of radial distance. See again the figure caption for details concerning the data set. The intensities show a sharp increase past the TS, peaking near the HP. The peak value seemingly depends on the HP position, and warrants further investigation. Note that the steep decrease at the HP is caused by the condition assumed at the HP. For an alternative scenario, see e.g. [6].

IV. Discussion and conclusions

From Figs. 4 and 5 the effects of adiabatic heating and stochastic acceleration in the heliosheath can clearly be seen: The O* intensities generally increase beyond the TS. Also, the spectra in the heliosheath are significantly effected, resulting in the observed modulated form. The computed O* intensities show very good agreement with Voyager 1 observations. However, the effect of time dependent modulation, through $\vec{K}(t)$, must still be evaluated. Notice also from Fig. 4 the difference between the modeled and observed O* cut-off intensities at $40 - 70$ MeV.nuc^{-1}. This is believed to be caused by the presence of multiple charged ACR, as discussed in [10].

The 1 AU values of K_P are also very high, but as shown by [9], the O* spectra at Earth remains unchanged by the inclusion of momentum diffusion, as spectra in the inner heliosphere are dominated by the $f \propto E^1$ adiabatic limit.

We conclude that a combination of diffusive acceleration, adiabatic heating and stochastic acceleration (the latter two occurring predominantly in the outer heliosheath) together form a viable process to explain the observed O* intensities in the heliosheath.

References

[1] Burger, R. A., *et al.* 2000. *J. Geophys. Res.*, 105(A12):27.
[2] Burger, R. A., *et al.* 2008. *Astrophys. J.*, 674:511.
[3] Ferreira, S. E. S., *et al.* 2007. *J. Geophys. Res.*, 112: A11101.
[4] Krimigis, S. M., *et al.* 1977. *Space Sci. Rev.*, 21:329.

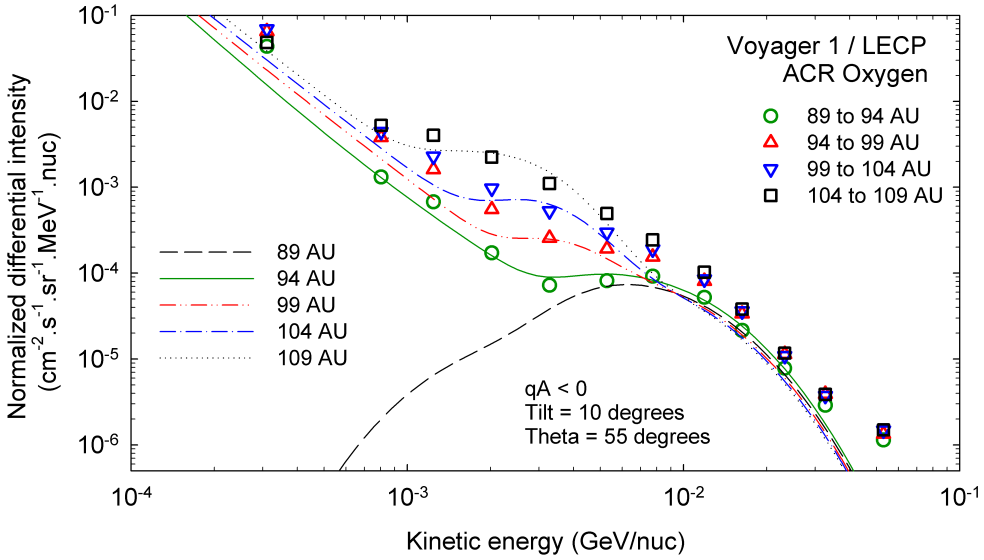

Fig. 4: Modeled O* spectra similar to Fig. 3, but shown at radial distances of 89, 94, 99, 104, 109 AU. The data consists of long term averages of O* energy spectra for four 5-AU-wide radial ranges (as shown), revealing the energetic particle behaviour at Voyager 1, upstream of the TS and in the heliosheath. Statistical uncertainties are not shown, but are smaller than the symbol size. Concerning the discrepancy between modeled and observational results above ~ 30 MeV.nuc^{-1}, see the accompanying paper [10].

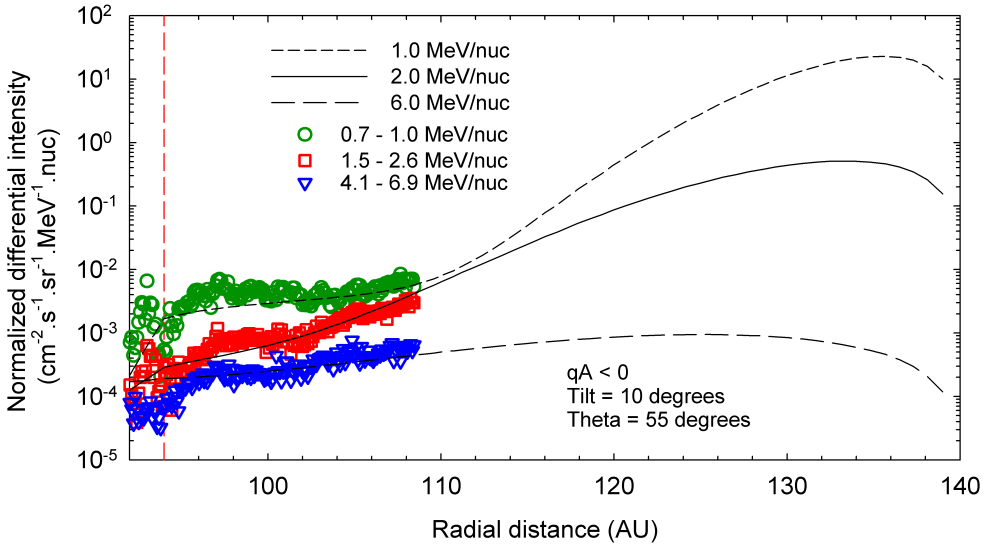

Fig. 5: The modeled O* intensities shown as a function of radial distance (mostly in the heliosheath) at energies of 1.0, 2.0 and 6.0 MeV.nuc^{-1}. The position of the TS is indicated by the vertical dashed line. Voyager 1 energetic O intensities are averaged over 0.10-AU-wide intervals and plotted against radial distance for three energy ranges (as shown). Statistical uncertainties are not shown, but are below approximately 10% after the TS crossing, 50% immediately upstream (e.g., late 2002) and 300% for > 1 MeV/nucleon ions well before the TS crossing (e.g., 2001).

[5] Langner, U. W., *et al.* 2006. *Astrophys. J.*, 640:1119.
[6] Scherer, K., *et al.* 2008. *Astrophys. J.*, 680:L105.
[7] Schlickeiser, R 2002. *Cosmic Ray Astrophysics*. Springer:Berlin.
[8] Stawicki, O. 2003. *Ph.D. Thesis*. University of Bochum.
[9] Strauss, R. D., *et al.* 2009a. *Modeling of Anomalous Cosmic Ray Oxygen in the Heliosphere. This conference*.
[10] Strauss, R. D., *et al.* 2009b. *The Acceleration and Modulation of Multiple Charged Anomalous Cosmic Rays Revisited. This conference.*
[11] Teufel, A. and Schlickeiser, R. 2003. *Astron. Astrophys.*, 397:15.
[12] Webber, W. R., *et al.* 2007. *J. Geophys. Res.*, 112:A06105.
[13] Zhang, M. 2006. *Physics of the Inner Heliosheath*, 858:226.